

# Optical investigation of monolayer and bulk tungsten diselenide ( $\text{WSe}_2$ ) in high magnetic fields

A. A. Mitioglu,<sup>†,||</sup> P. Plochocka,<sup>\*,†</sup> Á. Granados del Aguila,<sup>‡</sup> P. C. M. Christianen,<sup>‡</sup>  
G. Deligeorgis,<sup>¶</sup> S. Anghel,<sup>§</sup> L. Kulyuk,<sup>§</sup> and D. K. Maude<sup>†</sup>

*Laboratoire National des Champs Magnétiques Intenses, CNRS-EMFL-UJF-UPS-INSA, Grenoble and Toulouse, France, High Field Magnet Laboratory (HFML - EMFL), Institute for Molecules and Materials, Radboud University, Toernooiveld 7, 6525 ED NIJMEGEN, The Netherlands, FORTH-IESL, Microelectronics Research Group, P.O. Box 1527, 71110 Heraklion, Crete, Greece, and Institute of Applied Physics, Academiei Str. 5, Chisinau, MD-2028, Republic of Moldova*

E-mail: paulina.plochocka@lncmi.cnrs.fr

## Abstract

Optical spectroscopy in high magnetic fields  $B \leq 65$  T is used to reveal the very different nature of carriers in monolayer and bulk transition metal dichalcogenides. In monolayer  $\text{WSe}_2$ , the exciton emission shifts linearly with the magnetic field and exhibits a splitting which originates from the magnetic field induced valley splitting. The monolayer data can be described using a single particle picture with a Dirac-like Hamiltonian for massive Dirac fermions, with

---

\*To whom correspondence should be addressed

<sup>†</sup>Laboratoire National des Champs Magnétiques Intenses, CNRS-EMFL-UJF-UPS-INSA, Grenoble and Toulouse, France

<sup>‡</sup>High Field Magnet Laboratory (HFML - EMFL), Institute for Molecules and Materials, Radboud University, Toernooiveld 7, 6525 ED NIJMEGEN, The Netherlands

<sup>¶</sup>FORTH-IESL, Microelectronics Research Group, P.O. Box 1527, 71110 Heraklion, Crete, Greece

<sup>§</sup>Institute of Applied Physics, Academiei Str. 5, Chisinau, MD-2028, Republic of Moldova

<sup>||</sup>Institute of Applied Physics, Academiei Str. 5, Chisinau, MD-2028, Republic of Moldova

an additional term to phenomenologically include the valley splitting. In contrast, in bulk WSe<sub>2</sub> where the inversion symmetry is restored, transmission measurements show a distinctly excitonic behavior with absorption to the 1s and 2s states. Magnetic field induces a spin splitting together with a small diamagnetic shift and cyclotron like behavior at high fields, which is best described within the hydrogen model.

Keywords: Transition metal dichalcogenides, WSe<sub>2</sub>, monolayer, bulk, massive Dirac fermions, Fermi velocity, valley splitting

Transition metal dichalcogenides (TX<sub>2</sub>, T=Mo,W,.. and X=S, Se,..) are quasi two dimensional layered materials with strong ionic-covalent bonding within a layer. A monolayer is composed of a single layer of transition metal embedded between two atomic layers of chalcogenides atoms in a trigonal prismatic structure. The weak van der Waals interlayer coupling nevertheless completely modifies the band structure. Bulk crystals are indirect semiconductors with extremely weak phonon assisted photoluminescence (PL) emission. In monolayer TX<sub>2</sub> the inversion symmetry is broken as the two sublattices are occupied by one T atom and two X<sub>2</sub> atoms. The band gap is direct and located in two degenerate valleys ( $K\pm$ ) at the corner of hexagonal Brillouin zone and the PL emission has a quantum yield which is four orders of magnitude larger than that of bulk crystals.<sup>1-6</sup> In addition, dielectric confinement, due to the very different dielectric environment outside of the monolayer, enhances the exciton binding energy beyond the usual factor of four limit for two-dimensional systems.<sup>7,8</sup>

Due to the  $d$  character of the orbitals, these materials exhibits a strong spin orbit coupling,<sup>9</sup> which when combined with the lack of inversion and time reversal symmetry, breaks the spin degeneracy and leads to a strong spin orbit induced Zeeman effect.<sup>4,10</sup> Hence, the spin and valley degrees of freedom are coupled which in turn leads to the valley contrasting selection rules for optical interband transitions with circularly polarized light:<sup>11,12</sup>  $\sigma^+$  couples to the  $K^+$  valley and  $\sigma^-$  to  $K^-$  respectively (see inset in Fig 1). Significant valley polarization was reported recently for monolayer MoS<sub>2</sub> and WSe<sub>2</sub>.<sup>13-15</sup> Amongst the transition metal dichalcogenides, WSe<sub>2</sub> has the most robust valley polarization, essentially due to the very large spin orbit splitting in the valence

band of this material.<sup>13</sup>

In transition metal dichalcogenides, the valley degree of freedom can be manipulated and potentially can be used to replace charge for the transmission of information.<sup>11–13,15–19</sup> For example, the anomalous Hall effect, whose sign depends on the valley index, was recently demonstrated<sup>20,21</sup> and an external magnetic field can be used to tune the valley and spin polarization.<sup>22</sup> To date, the valley splitting has been investigated for WSe<sub>2</sub> and MoSe<sub>2</sub> in only moderately low magnetic fields  $B \leq 10$  T.<sup>22–25</sup>

In this letter we compare the optical response of monolayer and bulk WSe<sub>2</sub> in high magnetic fields up to  $B = 65$  T. We show that in monolayer WSe<sub>2</sub> both the exciton and the trion exhibits a splitting which originates from the lifting of the valley degeneracy in a magnetic field. The magnetic field has little effect on the valley polarization of the neutral exciton, whereas it can significantly increase or decrease the valley polarization of the trion depending on the circular polarization of the excitation light. The linear evolution of the energy of the exciton and trion features in magnetic field can be described using a Dirac-like Hamiltonian for massive Dirac fermions. In contrast, in bulk WSe<sub>2</sub> where the inversion symmetry is restored, we see excitonic behavior with absorption to the 1s and 2s hydrogen like states. Both states show a spin (Zeeman) splitting accompanied by a small diamagnetic shift at low magnetic fields before shifting as the cyclotron energy in the high field limit.

For the measurements, single layer flakes of tungsten diselenide (WSe<sub>2</sub>) have been obtained by mechanical exfoliation of bulk 2H-WSe<sub>2</sub> (the hexagonal 2H-polytype of tungsten diselenide) single crystals grown using chemical vapor transport with Bromine as the transport agent. Samples obtained in this way are naturally n-type.<sup>26</sup> Two types of experiments have been performed; (i) micro-photoluminescence ( $\mu$ PL) on direct gap monolayer WSe<sub>2</sub> in steady state magnetic field up to 30 T and (ii) macro transmission of thin crystals of indirect gap bulk WSe<sub>2</sub> in the pulsed magnetic field up to 65 T. Combining PL and transmission allows us to probe the A-exciton of an electron-hole pair at the K-points of the Brillouin zone in both monolayer and in bulk WSe<sub>2</sub> for which PL is dominated by the indirect gap.

For  $\mu$ PL measurements the  $\text{WSe}_2$  monolayer flake was placed in a system composed of piezo-electric  $x - y - z$  translation stages and a microscope objective. The  $\mu$ PL system was cooled in exchange gas to a temperature of  $T=4.2$  K in a cryostat filled with liquid helium which was placed in a resistive magnet producing magnetic fields up to  $B = 30$  T. The magnetic field was applied in the Faraday configuration and the sample was illuminated by a laser at 640 nm. The excitation power was kept low (of the order of a few hundred of nW) to avoid heating effects. Both the exciting and collected light were transmitted through a non polarizing cube beam splitter (50:50) placed on the optical axis of the objective. With this setup the circular polarization of the excitation and detection can be controlled independently. The diameter of the excitation beam on the sample was of the order of  $1 \mu\text{m}$ .

The magneto-transmission measurements were performed on thin bulk samples (also obtained by limited mechanical exfoliation) in pulsed fields  $\leq 65$  T ( $\simeq 400$  ms). A tungsten halogen lamp provides a broad spectrum in the visible and near infra-red range and the absorption is measured in the Faraday configuration with the  $c$ -axis of the sample parallel to magnetic field. Typical size of the spot was of the order of  $200 \mu\text{m}$  and the polarization optics was introduced in situ. The sample was immersed in a helium bath cryostat pumped to a temperature of  $\simeq 1.8$  K to avoid noise due to the formation of helium gas bubbles. Note, that we are unable to perform macro transmission measurements on monolayer  $\text{WSe}_2$  as only a tiny fraction of the transmitted light would pass through the micron size flake and our  $\mu$ PL setup is not adapted for micro-transmission measurements.

For both measurements the collected light was dispersed in a spectrometer equipped with a multichannel CCD camera cooled to liquid nitrogen temperatures.

Fig 1 shows a comparison between the emission spectra measured on a single layer flake and the transmission through the thin bulk crystals of the  $\text{WSe}_2$  all measured at zero magnetic field. In both spectra we observe a strong resonance around 1730 meV which corresponds well to the energy  $1s$  ( $n = 1$ ) state of the A-exciton, previously reported for monolayer<sup>13,27–29</sup> and bulk  $\text{WSe}_2$ .<sup>27,30</sup> The slightly higher energy of the A exciton emission observed in monolayer layer  $\text{WSe}_2$  (compared to

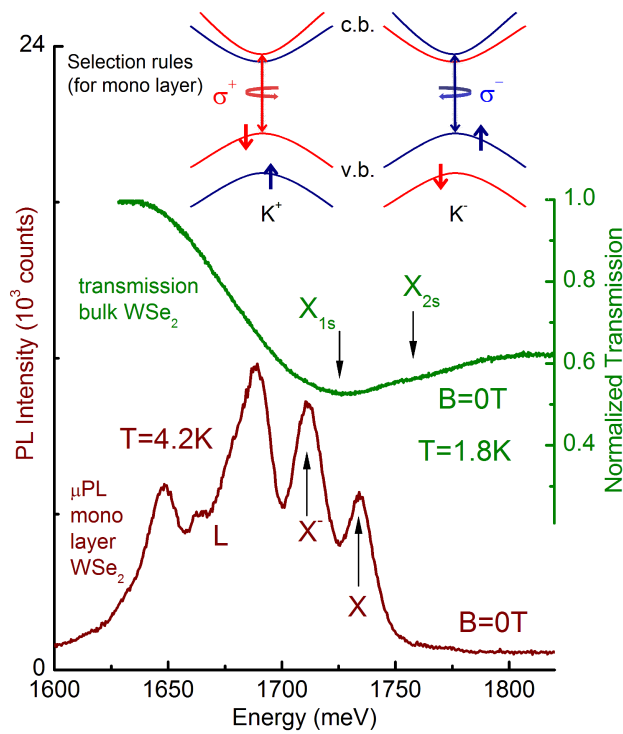


Figure 1: Typical low temperature  $\mu$ PL of monolayer and transmission spectra of bulk  $\text{WSe}_2$ . The inset illustrates the optical valley selection rules in monolayer  $\text{WSe}_2$  for  $\sigma^+$  and  $\sigma^-$  circular polarization of the photons (c.b. labels the conduction band and v.b. labels the valence band).

bulk transmission) is also in agreement with previous studies.<sup>27,28</sup> We also see the 2s ( $n = 2$ ) exciton level in transmission, previously reported in reflectance measurements.<sup>30</sup> The separation of the 1s and 2s transitions, equal to  $3R_y^*/4$  in the 3D hydrogen model ( $E_n = R_y^*/n^2, n = 1, 2, \dots$ ) provides a rough estimate for the exciton binding energy in bulk WSe<sub>2</sub> of  $R_y^* \approx 44$  meV. The monolayer emission spectrum has additional emission lines on the low energy side. The line around 30 meV lower than the exciton corresponds well to the negatively charged exciton (trion) emission, as our samples are naturally n-doped.<sup>26</sup> Trion emission is routinely observed in mono layers dichalcogenides with an excess concentration of electrons and can be unambiguously identified by its characteristic power dependence.<sup>31,32</sup> Moreover, the observed binding energy of the trion corresponds well to the experimental value previously reported for WSe<sub>2</sub>.<sup>13,29,33</sup> Below the trion emission several peaks are observed which we label as “L” as they can be assigned to localized (bound exciton) states previously reported in WSe<sub>2</sub> and MoS<sub>2</sub>.<sup>15,29,33</sup>

In the following we focus on the magnetic field dependence of the exciton transitions. Typical low temperature  $\mu$ PL spectra of monolayer WSe<sub>2</sub> measured in *dc* magnetic fields up to 30 T are presented in Fig 2(a). The results of the transmission measurements through the thin layers of bulk WSe<sub>2</sub> measured in pulsed magnetic fields up to 65 T are presented in Fig 2(b). For both data sets the solid and dotted lines correspond to  $\sigma^+$  and  $\sigma^-$  detection respectively. The photoluminescence was excited using  $\sigma^+$  polarization while for the transmission unpolarized white light was used for the excitation.

In both bulk and monolayer crystals the polarization resolved measurements reveal a splitting of the exciton transition, nevertheless with very different physical origins due to the markedly different optical selection rules in bulk and monolayer WSe<sub>2</sub>. Additionally, the monolayer emission shows that, already at zero magnetic field, both the neutral and charged exciton populations are partially valley polarized as the emission intensity is not the same for  $\sigma^+$  and  $\sigma^-$  detection. This is not surprising, as our circular excitation was relatively close to the exciton resonance, as also previously reported for WSe<sub>2</sub>.<sup>13</sup>

In monolayer WSe<sub>2</sub> the circular polarization  $\sigma^\pm$  of the excitation allows us to selectively pump

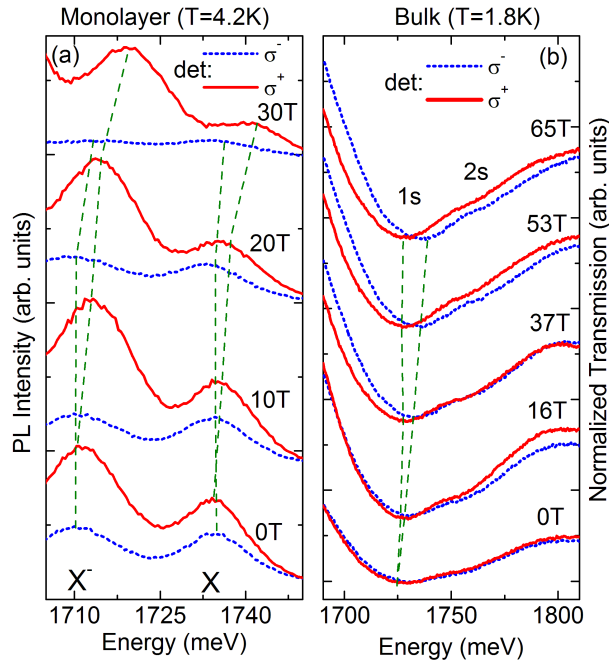


Figure 2: Typical low temperature spectra at various magnetic fields of (a)  $\mu$ PL from monolayer WSe<sub>2</sub> and (b) transmission through the thin WSe<sub>2</sub> bulk crystal, using  $\sigma^+$  and  $\sigma^-$  detection. For the PL shown here  $\sigma^+$  polarized light was used for excitation while the white light for the transmission measurements was unpolarized. The dashed lines are drawn as a guide for eye showing the evolution of exciton features with magnetic field. The spectra have been shifted vertically for clarity.

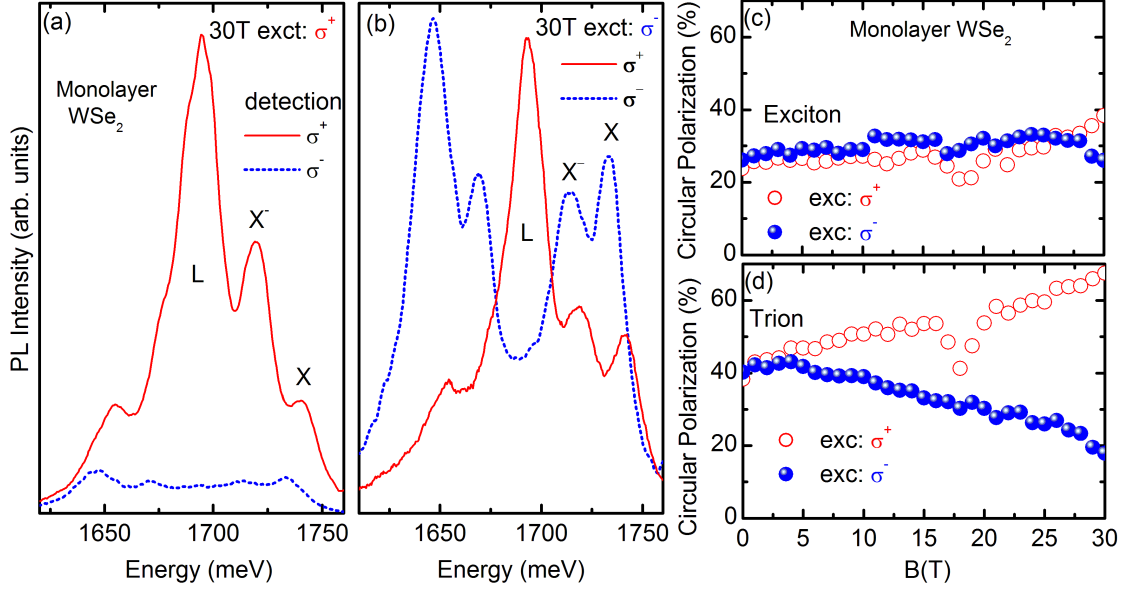


Figure 3: (a),(b) Typical  $\mu$ PL spectra excited  $\sigma^+$  and  $\sigma^-$  polarized laser respectively. The red/blue lines denote the detection in  $\sigma^+$  and  $\sigma^-$  respectively. (c),(d) degree of circular polarization of the neutral and charged exciton respectively. The open symbols denote  $\sigma^+$  excitation as closed one correspond to the  $\sigma^-$  polarization of the excitation.

the  $K^+$  or  $K^-$  valley. The circular polarization of the emission then depends on the inter valley scattering rate and the radiative recombination lifetime. In the absence of inter valley scattering the emission would be 100% polarized. The degree of circular polarization  $P$  for the exciton and trion emission can be defined as

$$P = \frac{I_{\sigma^+} - I_{\sigma^-}}{I_{\sigma^+} + I_{\sigma^-}}, \quad (1)$$

where  $I_{\sigma^\pm}$  is the intensity of the photoluminescence for a given circular (detection) polarization obtained by fitting the spectra with a Gaussian function for each value of magnetic field.

We have analyzed data for all four possible combinations of the circular polarization of the excitation and detection. Typical polarization resolved  $\mu$ PL spectra measured at 30 T for  $\sigma^+$  and  $\sigma^-$  are presented in Fig 3(a) and (b) respectively. Note that the direction of the magnetic field was the same for all measurements. The required polarization combination was selected by rotating the excitation and detection polarization optics located outside of the cryostat. As in zero field, the 30 T raw data clearly shows that both neutral and charge exciton exhibits a significant degree of



circular polarization.

The full magnetic field dependence of calculated degree of circular polarization of the neutral and charged exciton calculated using Equation 1 is presented in Fig 3(c),(d) respectively. Both neutral and charged exciton shows a valley polarization in zero magnetic field. For the exciton  $P = 25\%$  and for the charged exciton  $P = 40\%$ . Although we are not exciting exactly at the resonance it has been shown that  $\text{WSe}_2$ , which has the largest spin orbit induced spin splitting in both valence and the conduction bands of any member of the  $\text{TX}_2$  family, has a valley polarization which is the most robust of all the transition metal dichalcogenides.<sup>13</sup> For the exciton the degree of the circular polarization remains almost unchanged with the magnetic field suggesting that magnetic field has little influence on the inter valley exciton scattering rate. On the other hand the degree of polarization is trion is strongly influenced with the polarization of the  $\sigma^+$  excited emission (pumping K+ valley) increasing strongly, accompanied by an equally strong reduction in the degree of polarization for  $\sigma^-$  excitation (pumping K- valley). This suggests, that although the magnetic field does not modify the inter valley exciton scattering rate, it can nevertheless modify the probability for trion formation, most likely via its influence on the excess electron population of the spin orbit split spin levels in the conduction band for each valley.

The evolution of the exciton and trion polarization reported here is somewhat different from previous investigations of  $\text{WSe}_2$ <sup>22</sup> and  $\text{MoSe}_2$ <sup>23</sup> which might be due to the low magnetic fields employed ( $B \leq 7$  T). For example, in our data, the true behavior of the trion polarization is only revealed for magnetic fields  $B \geq 5$  T. Additionally, the polarization depends sensitively upon the exact excitation used, together with sample dependent parameters such as the valley scattering rate.

The energy of the polarization resolved exciton and trion emission for monolayer  $\text{WSe}_2$  is shown in figure 4(a). Both the exciton and trion energy shifts linearly to higher energy with increasing magnetic field showing a pronounced splitting which also evolves linearly with magnetic field. In the transition metal dichalcogenides the carriers behave as massive Dirac fermions which can be described by a Dirac like Hamiltonian.<sup>11,34</sup> In this simple picture the magnetic field quan-

tizes the energy of the carriers in the conduction and valence bands into Landau levels with energy,

$$E_{\lambda}^{\pm K} = \lambda \sqrt{\Delta^2 + n\varepsilon^2} \pm \frac{1}{2}g_v\mu_B B, \quad (2)$$

where  $\lambda = \pm 1$  designates the conduction/valence band,  $\Delta$  is half of the band gap and  $\varepsilon = \sqrt{2}\hbar v_F/\ell_B$  is the characteristic magnetic energy. Here  $n$  is the Landau level index,  $v_F$  is the Fermi velocity and  $\ell_B = (\hbar/eB)^{1/2}$  is the magnetic length. Note in this single particle picture  $2\Delta$  is obtained from the observed zero magnetic field transition energy to which the exciton binding energy in monolayer WSe<sub>2</sub> of  $E_B = 370$  meV has to be added.<sup>35</sup>

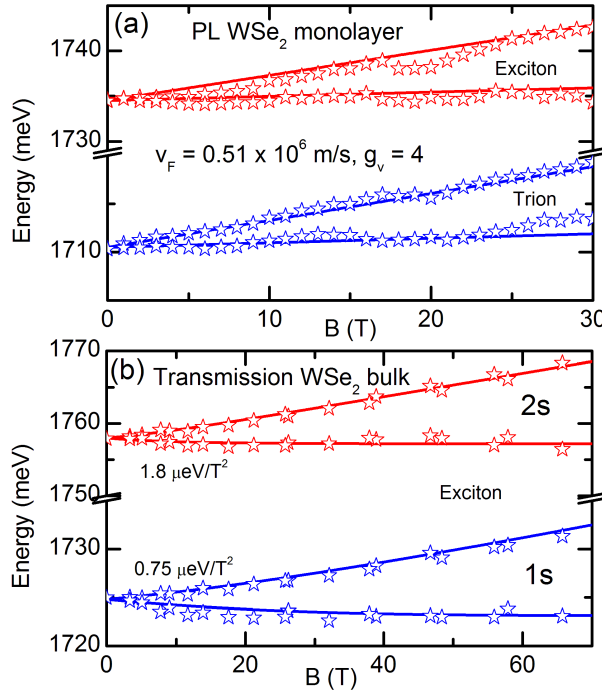


Figure 4: (a) Magnetic field dependence of the energy of the polarization resolved exciton emission in monolayer WSe<sub>2</sub> measured at  $T = 4.2$  K. The solid lines are fits to the data using the Hamiltonian for massive Dirac fermions. (b) Magnetic field dependence of transmission in bulk WSe<sub>2</sub> measured at  $T = 1.8$  K. The solid lines are fits to the data using Equation 3 to model the diamagnetic (quadratic) shift at low magnetic fields followed by a linear Landau like behavior at high magnetic fields.

As in graphene, in the transition metal dichalcogenides the selections rules for dipole allowed optical transitions are  $\Delta n = \pm 1$ , *i.e.* the Landau level index changes by one. In this case spin is

conserved and any spin splitting of the Landau levels will not give rise to a splitting of the optical transition unless the electron and hole g-factors are significantly different. Thus, the observed splitting of the transitions is included simply as a phenomenological valley splitting  $\pm \frac{1}{2} g_v \mu_B B$  where  $g_v$  is the effective valley g-factor. The  $n > 0$  Landau levels always occur in pairs with one in each valley in both the conduction and valence bands. The  $n = 0$  level is special and there is a single  $n = 0$  Landau level per valley. For both spin levels, the  $n = 0$  Landau level is fixed at the top of the valence band for the  $+K$  valley and at the bottom of the conduction band for the  $-K$  valley.<sup>34</sup> Thus, in a magnetic field resonant  $\sigma^\pm$  excitation selects  $0 \rightarrow 1$  or  $1 \rightarrow 0$  optical transitions and therefore selecting the valley as in the zero magnetic field case (see schematic in Figure 5).

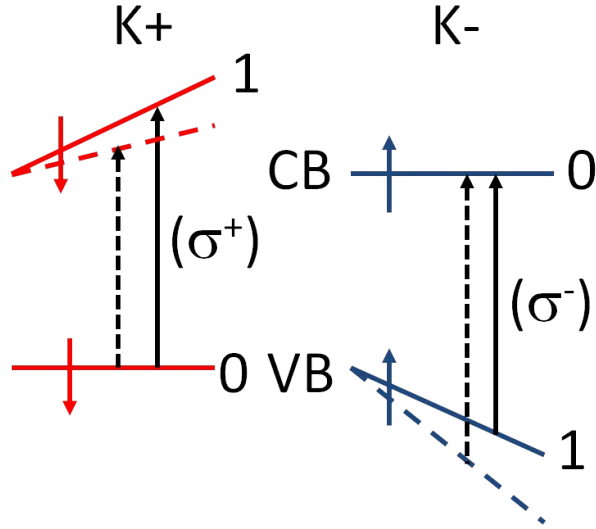


Figure 5: Schematic showing evolution of the  $n = 0, 1$  Landau levels of massive Dirac fermions in a magnetic field together with the dipole allowed  $0 \rightarrow 1$  and  $1 \rightarrow 0$  transitions which select the valley involved (solid lines are Landau levels, solid arrows indicate the transitions). Spin is conserved so that the Zeeman energy (not shown here) does not split the transition. Any asymmetry of the electron/hole Dirac cones, which modifies the energy of the  $n = 1$  Landau levels, would split the transition as indicated by the dashed lines/arrows.

The solid lines in figure 4(a) are the transitions energies calculated from the energies of the  $0 \rightarrow 1$  and  $1 \rightarrow 0$  transitions from Equation 2 with a Fermi velocity  $v_F = (0.51 \pm 0.02) \times 10^6$  m/s and an effective valley g-factor  $g_v = 4 \pm 0.5$ . We have included excitonic effects simply by subtracting the exciton (trion) binding energy from the calculated transition energy. The parameter set provides a

reasonable fit to both the exciton and trion emission data. The transition energies evolve linearly with magnetic field which can be understood as follows: The band gap of WSe<sub>2</sub> is large so that for the magnetic fields of interest here  $\Delta^2 \gg \varepsilon^2$  so that the orbital contribution to the Landau level energy is well approximated by a Taylor expansion

$$E_n = \pm\Delta(1 + n\varepsilon^2/\Delta^2)^{\frac{1}{2}} \simeq \pm(\Delta + n\hbar eBv_F^2/\Delta).$$

Thus, the carriers behave as massive Dirac fermions with an effective mass  $m^* = \Delta/v_F^2 \simeq 0.7m_e$  where  $m_e$  is the free electron mass. Note, that this result can also be obtained by comparison with the Klein-Gordon equation  $E^2 = m^2c^4 + p^2c^2$  replacing the speed of light with the Fermi velocity. For this reason  $\Delta \equiv mc^2$  is often referred to as the “mass gap”.

The observed splitting is asymmetric due to the orbital (Landau level) contribution which is always positive. The low energy peak almost does not move in magnetic field as the orbital and valley contributions are of similar size but of opposite sign. Li et al.<sup>25</sup> observe a similar valley splitting in MoSe<sub>2</sub> of 0.24meV/T but with a symmetric splitting in fields up to 10T. This may suggest that the orbital contribution is quenched in their measurements, either due to the higher temperature used ( $T = 10$  K) or increased disorder in their sample ( $\omega_c\tau < 1$ ).

In the literature the splitting of the transition is often described, using slightly different language, in terms of a two band tight binding model in which the atomic  $d$ -orbitals which form the valence band have an in plane angular momentum  $m\hbar$  with  $m = \pm 2$  according to the valley index. In magnetic field, the valley splitting is then  $4\mu_B B$  which agrees within error with the splitting observed here (we estimate from the fit that  $g_v = 4.0 \pm 0.5$ ). From low field measurements ( $B < 10T$ ) Srivastava and co-workers find a similar value for the valley splitting of WSe<sub>2</sub> ( $g_v = 4.3$ ),<sup>24</sup> while a factor of two lower value ( $\simeq 2\mu_B B$ ) has been published recently by Aivazian and co-workers.<sup>22</sup> In the tight binding model, the valley magnetic moment due to the self rotation of the wave packet gives no contribution to the splitting provided the electron and hole masses are identical. Aivazian *et al.*<sup>22</sup> invoked different electron and hole masses to correctly predict the observed splitting in

their samples. Similarly, in our Hamiltonian any asymmetry of the electron and hole Dirac cones would lead to a splitting of the  $0 \rightarrow 1$  and  $1 \rightarrow 0$  transitions (see Figure 5). However, as our data corresponds within error to the expected splitting of  $4\mu_B B$ , this suggest that electron-hole asymmetry in WSe<sub>2</sub> is small and makes no significant contribution to the observed valley splitting.

For bulk WSe<sub>2</sub>, the dipole selection rules are  $\Delta n = 0$  so that the angular momentum of the photon is used to flip the spin. The energy of the polarization resolved exciton features in transmission for bulk WSe<sub>2</sub> shown in figure 4(b) clearly shows signs of excitonic effects with quadratic diamagnetic shift at low magnetic fields which becomes more linear at high fields. The evolution of the data in magnetic field can be well described using

$$\Delta E_{\uparrow\downarrow} = -\frac{\hbar\omega_0}{2} + \frac{\hbar}{2}\sqrt{\omega_0^2 + \omega_c^2} \pm \frac{1}{2}g_s\mu_B B, \quad (3)$$

where  $\hbar\omega_0$  is an energy which controls the diamagnetic shift,  $\hbar\omega_c = eB/m^*$  is the cyclotron energy and  $m^*$  is the reduced exciton mass. The observed spin splitting is included via an effective g-factor  $g_s$ .

Neglecting spin for the moment, at high magnetic field  $\omega_c^2 \gg \omega_0^2$  and the energy is well approximated by  $\hbar\omega_c/2$ . At low fields when  $\omega_0^2 \gg \omega_c^2$  to first order a Taylor expansion gives the diamagnetic shift

$$\Delta E \simeq \frac{\hbar e^2 B^2}{4\omega_0 m^{*2}} = e^2 a_0^2 B^2.$$

Here we have defined a length  $a_0 = \sqrt{\hbar/4m^{*2}\omega_0}$  which can be identified with the effective Bohr radius in the hydrogen model.

The solid lines in figure 4(b) are the transition energies calculated using Equation 3. For the 1s absorption, we use an effective mass  $m^* = 0.7m_e$  as in monolayer WSe<sub>2</sub>. The spin splitting can be reproduced using an effective g-factor  $g_s = 2.3$  and the diamagnetic shift reproduced using  $\hbar\omega_0 = 8$  meV. This gives an estimation of the diamagnetic shift at low magnetic fields of  $\Delta E \approx 0.9\mu\text{V/T}^2$ . The effective Bohr radius is  $a_0 \approx 1.8$  nm from which we can obtain a rough estimate of the exciton binding energy in the hydrogen model  $e^2/8\pi\epsilon_r\epsilon_0 a_0 \approx 56$  meV using a dielectric constant  $\epsilon_r \simeq 7$  for

bulk 2H-WSe<sub>2</sub>. This value agrees well with the exciton binding energy of  $\simeq 55$  meV determined directly from the  $n = 1, 2, 3$  hydrogen series of levels in reflectance measurements on bulk 2H-WSe<sub>2</sub> crystals.<sup>30</sup> A similar binding energy ( $\simeq 56$  meV) has been reported<sup>36</sup> in high magnetic field measurements up to 150 T on bulk MoS<sub>2</sub>, however with a much smaller diamagnetic shift  $\simeq 0.2 \mu\text{eV/T}^2$ . The approximately four fold smaller diamagnetic shift is however, fully consistent with our data on WSe<sub>2</sub> when the smaller Bohr radius (1.28 nm) and smaller reduced exciton mass ( $0.4m_e$ ) in MoS<sub>2</sub> are taken into account.<sup>36</sup>

For completeness, we have also fitted the 2s data using the same effective mass  $m^* = 0.7m_e$ , a slightly larger effective g-factor is required  $g_s = 2.8$ , with a smaller value of  $\hbar\omega_0 = 2$  meV. The estimated diamagnetic shift  $\Delta E \approx 3.4 \mu\text{V/T}^2$  is larger due to the more delocalized nature of the 2s wave function which extends over  $\approx 3.7$  nm.

In conclusion, we have investigated monolayer and bulk WSe<sub>2</sub> in high magnetic fields up to  $B = 65$  T using optical spectroscopy. In monolayer WSe<sub>2</sub>, the exciton emission exhibits a splitting which originates from lifting of the valley degeneracy by the magnetic field. The linear evolution of the energy of the exciton features in magnetic field can be described using a Dirac-like Hamiltonian for massive Dirac fermions with a Fermi velocity of  $0.51 \times 10^6$  m/s and an effective valley g-factor  $g_v = 4$  for an assumed effective spin  $s = 1/2$  system. The measured Fermi velocity can be used to estimate the effective hopping integral  $t$  of the tight binding Hamiltonian using  $at = \hbar v_F$  where  $a = 3.31$ . The measured value of  $\hbar v_F = 3.36$  eV suggests  $t = 1.02$  eV which is roughly 15% less than the effective hopping integral predicted from first principle band structure calculations.<sup>11,34</sup> In contrast, in bulk WSe<sub>2</sub> where the inversion symmetry is restored, transmission measurements show that the exciton exhibits a spin (Zeeman) splitting and the exciton 1s and 2s features show a small diamagnetic shift which allows us to determine the exciton binding energy of around 56 meV within the three dimensional hydrogen model. In two dimensions, the binding energy is enhanced by at most a factor of four, so the predicted 2D exciton binding energy ( $4 \times 56 \approx 224$  meV) is significantly less than the established value of 370 meV in monolayer WSe<sub>2</sub>.<sup>30</sup> This suggests that dielectric screening (image charge), due to the very different dielectric environment outside of

the material,<sup>7,8</sup> significantly enhances the exciton binding energy in monolayer transition metal dichalcogenides.

## Acknowledgement

This work was partially supported by Programme Investissements d’Avenir under the program ANR-11-IDEX-0002-02 - reference ANR-10-LABX-0037-NEXT, ANR JCJC project milliPICS, the Region Midi-Pyrénées under contract MESR 13053031 , and STCU project 5809, We also acknowledge the support of HFML-RU/FOM, member of the European Magnetic Field Laboratory (EMFL) and support by EuroMagNET II under the EU Contract Number 228043. One of us (A.A.M.) was partially supported during his visit to HMFL to perform these measurements by a “Bourse d’excellence EOLE du Réseau franco-néerlandais”. Finally, it is our pleasure to thank S. George for her technical assistance with the pulsed field transmission measurements.

## Supporting Information Available

Four figures in which Gaussians are fitted to the raw data to extract the energy of the exciton and trions features are available as supplementary information.

## References

- (1) Albe, K.; Klein, A. *Phys. Rev. B* **2002**, *66*, 073413.
- (2) Mak, K. F.; Lee, C.; Hone, J.; Shan, J.; Heinz, T. F. *Phys. Rev. Lett.* **2010**, *105*, 136805.
- (3) Splendiani, A.; Sun, L.; Zhang, Y.; Li, T.; Kim, J.; Chim, C.-Y.; Galli, G.; Wang, F. *Nano Letters* **2010**, *10*, 1271–1275.
- (4) Cheiwchanchamnangij, T.; Lambrecht, W. R. *Phys. Rev. B* **2012**, *85*, 205302.
- (5) Ramasubramaniam, A. *Phys. Rev. B* **2012**, *86*, 115409.

- (6) Zhao, W.; Ribeiro, R. M.; Toh, M.; Carvalho, A.; Kloc, C.; Castro Neto, A. H.; Eda, G. *Nano Letters* **2013**, *13*, 5627–5634.
- (7) Lin, Y.; Ling, X.; Yu, L.; Huang, S.; Hsu, A. L.; Lee, Y.-H.; Kong, J.; Dresselhaus, M. S.; Palacios, T. *Nano Letters* **2014**, *14*, 5569–5576.
- (8) Chernikov, A.; Berkelbach, T. C.; Hill, H. M.; Rigosi, A.; Li, Y.; Aslan, O. B.; Reichman, D. R.; Hybertsen, M. S.; Heinz, T. F. *Phys. Rev. Lett.* **2014**, *113*, 076802.
- (9) Mattheiss, L. *Phys. Rev. B* **1973**, *8*, 3719–3740.
- (10) Zhu, Z.; Cheng, Y.; Schwingenschlögl, U. *Phys. Rev. B* **2011**, *84*, 153402.
- (11) Xiao, D.; Liu, G.-B.; Feng, W.; Xu, X.; Yao, W. *Phys. Rev. Lett.* **2012**, *108*, 196802.
- (12) Yao, W.; Xiao, D.; Niu, Q. *Phys. Rev. B* **2008**, *77*, 235406.
- (13) Jones, A. M.; Yu, N. J., Hongyi and Ghimire; Wu, S.; Aivazian, G.; Ross, J. S.; Zhao, B.; Yan, J.; Mandrus, D. G.; Xiao, D.; Yao, W.; Xu, X. *Nature Nanotechnology* **2013**, *8*, 634.
- (14) Cao, T.; Wang, G.; Han, W.; Ye, H.; Zhu, C.; Shi, J.; Niu, Q.; Tan, P.; Liu, E. W. B.; Feng, J. *Nature Communications* **2012**, *3*, 887.
- (15) Mak, K. F.; He, K.; Shan, J.; Heinz, T. F. *Nature Nanotechnology* **2012**, *7*, 494.
- (16) Xu, X.; Yao, W.; Xiao, D.; Heinz, T. F. *Nature Physics* **2014**, *10*, 343.
- (17) Suzuki, R.; Sakano, M.; Zhang, Y. J.; Akashi, R.; Morikawa, D.; Harasawa, A.; Yaji, K.; Kuroda, K.; Miyamoto, K.; Okuda, T.; Ishizaka, K.; Arita, R.; Iwasa, Y. *Nature Nanotechnology* **2014**, *9*, 611.
- (18) Behnia, K. *Nature Nanotechnology* **2012**, *7*, 488.
- (19) Nebel, C. E. *Nature Materials* **2013**, *12*, 690.



- (20) Wu, S.; Ross, J. S.; Liu, G.-B.; Aivazian, G.; Jones, A.; Fei, Z.; Zhu, W.; Xiao, D.; Yao, W.; Cobden, D.; Xu, X. *Nature Physics* **2013**, *9*, 149–153.
- (21) Mak, K. F.; McGill, K. L.; Park, J.; McEuen, P. L. *Science* **2014**, *344*, 1489–1492.
- (22) Aivazian, G.; Gong, Z.; Jones, A. M.; Chu, R.-L.; Yan, J.; Mandrus, D. G.; Zhang, C.; Cobden, D.; Yao, W.; Xu, X. *Nature Physics* **2015**, *11*, 148.
- (23) MacNeill, D.; Heikes, C.; Mak, K. F.; Anderson, Z.; Kormányos, A.; Zólyomi, V.; Park, J.; Ralph, D. C. *Phys. Rev. Lett.* **2015**, *114*, 037401.
- (24) Srivastava, A.; Sidler, M.; Allain, A. V.; Lembke, D. S.; Kis, A.; Imamoglu, A. *Nature Physics* **2015**, *11*, 141.
- (25) Li, Y.; Ludwig, J.; Low, T.; Chernikov, A.; Cui, X.; Arefe, G.; Kim, Y. D.; van der Zande, A. M.; Rigosi, A.; Hill, H. M.; Kim, S. H.; Hone, J.; Li, Z.; Smirnov, D.; Heinz, T. F. *Phys. Rev. Lett.* **2014**, *113*, 266804.
- (26) El-Mahalawy, S. H.; Evans, B. L. *Phys. Status Solidi B* **1977**, *79*, 713.
- (27) Zeng, H.; Liu, G.-B.; Dai, J.; Yan, Y.; Zhu, B.; He, R.; Xie, L.; Xu, S.; Chen, X.; Yao, W.; Cui, X. *Scientific Reports* **2013**, *3*, 1608.
- (28) Zhao, W.; Ghorannevis, Z.; Chu, L.; Toh, M.; Kloc, C.; Tan, P.-H.; Eda, G. *ACS Nano* **2013**, *7*, 791–797.
- (29) Wang, G.; Bouet, L.; Lagarde, D.; Vidal, M.; Balocchi, A.; Amand, T.; Marie, X.; Urbaszek, B. *Phys. Rev. B* **2014**, *90*, 075413.
- (30) Beal, A. R.; Liang, W. Y. *Journal of Physics C: Solid State Physics* **1976**, *9*, 2459.
- (31) Mak, K. F.; He, K.; Lee, C.; Lee, G. H.; Hone, J.; Heinz, T. F.; Shan, J. *Nature Materials* **2013**, *12*, 207–211.

- (32) Mitioğlu, A. A.; Plochocka, P.; Jadczyk, J. N.; Escoffier, W.; Rikken, G. L. J. A.; Kulyuk, L.; Maude, D. K. *Phys. Rev. B* **2013**, *88*, 245403.
- (33) Zhu, C. R.; Zhang, K.; Glazov, M.; Urbaszek, B.; Amand, T.; Ji, Z. W.; Liu, B. L.; Marie, X. *Phys. Rev. B* **2014**, *90*, 161302.
- (34) Rose, F.; Goerbig, M. O.; Piéchon, F. *Phys. Rev. B* **2013**, *88*, 125438.
- (35) He, K.; Kumar, N.; Zhao, L.; Wang, Z.; Mak, K. F.; Zhao, H.; Shan, J. *Phys. Rev. Lett.* **2014**, *113*, 026803.
- (36) Goto, T.; Kato, Y.; Uchida, K.; Miura, N. *Journal of Physics: Condensed Matter* **2000**, *12*, 6719.

This material is available free of charge via the Internet at <http://pubs.acs.org/>.